IEEE Access
Multidisciplinary ⋮ Rapid Review ⋮ Open Access Journal

Received February 23, 2021, accepted March 12, 2021, date of publication March 17, 2021, date of current version March 29, 2021.

Digital Object Identifier 10.1109/ACCESS.2021.3066475

Multi-Response Weighted Adaptive Sampling Approach Based on Hybrid Surrogate Model

JIANGQI LONG, YAOQING LIAO, AND PING YU
School of Mechanical and Electrical Engineering, Wenzhou University, Wenzhou 325035, China

Corresponding author: Ping Yu (yuping55@zju.edu.cn)

This work was supported in part by the National Natural Science Foundation of China under Grant 51475336 and Grant 51905383, in part by the Zhejiang Provincial Natural Science Foundation of China under Grant LGF21E050001, and in part by the Wenzhou Municipal Scientific Research Project of China under Grant G2020012.

ABSTRACT In order to improve the fitting accuracy and optimization efficiency of the surrogate model, a multi-response weighted adaptive sampling (MWAS) approach based on the hybrid surrogate model was proposed and implemented to a multi-objective lightweight design of car seats. In this approach, the sample discreteness index in the input design space was calculated by the maximum and minimum distance approach (MDA), the fitting uncertainty index of output response was calculated by a strategy based on the weighted prediction variance (WPV), and the two indices are combined by the weight coefficients. In the iterative process, the weight coefficients of the two indices were determined according to the accuracy of the hybrid surrogate model. The balance of global and local accuracy was realized by considering the sample dispersion and the fitting uncertainty of the surrogate model comprehensively. Numerical examples of single-response and multi-response systems showed that the proposed approach has excellent sampling efficiency and robustness. Moreover, the results of actual engineering application showed that the hybrid surrogate model constructed through MWAS could significantly improve the efficiency of model optimization. Hence, a high-precision optimization solution to the multi-objective lightweight design of passenger car rear seat was obtained.

INDEX TERMS Adaptive sampling, hybrid surrogate model, multi-objective lightweight, multi-response systems.

I. INTRODUCTION

Safety, energy conservation and environmental friendliness are the three major themes of the development of the automobile industry. While lightweight is one of the most important means to achieve these goals. Researchers all over the world have made tremendous efforts on this aspect [1]–[4]. However, in the field of automobile lightweight design, there is little research on passenger car rear seats. Therefore, it is of great significance to reduce the weight of the passenger car rear seat for the development of the automobile industry while satisfying the safety performance and riding comfort [5].

With the rapid development of computer hardware and software, high-fidelity simulations are often used to replace real-life experiments to reduce the overall time and cost. However, the simulation for a complex system with high dimensional and multi-output is computationally expensive. A widely used strategy is to utilize surrogate models and replace the expensive simulation model during the process. Various types of optimization designs (multi-objective optimization, reliability-based design optimization, and multidisciplinary design optimization) can be carried out quickly and conveniently, based on surrogate models and optimization algorithms [6]. Currently, mainstream surrogate models such as Polynomial Response Surface (PRS) models, Kriging (KRG) models, Radial Basis Function (RBF) models, and Elliptic Base Function (EBF) models have been widely applied to engineering optimization and achieved greater successes [7]–[12]. However, when solving multi-objective optimization problems with high dimensions and high degree of nonlinearity, it is difficult to obtain reasonably optimized results while relying only on a single surrogate model [13]. To solve this problem, Zerpa *et al.* [14] have first proposed the concept of a hybrid surrogate model and then applied it to alkaline surfactant polymer flooding to improve oil recovery. Chen *et al.* [15] and Zhang *et al.* [16] have proposed a new hybrid surrogate model which combined the advantages of global and local measures, and the appropriate trade-off between the two measures was made through the weight coefficients. Similarly, Yin *et al.* [17] have proposed a multi-region optimization hybrid surrogate model, which was

The associate editor coordinating the review of this manuscript and approving it for publication was Xiaosong Hu.

applied to two engineering examples of thin-walled column crushing and airbag buffering. The results showed that the prediction accuracy of the hybrid surrogate model proposed in the above literatures was higher than other single surrogate models.

In the field of multi-objective engineering optimization research, the accuracy of the surrogate model largely depends on the number of sample points and their location distribution on the design space [18]. Therefore, the distribution of the sample points in a reasonable location has become the key factor for engineering optimization. At present, there are mainly two types of sample techniques. The one-time sampling approach generates all sample points at one time through experimental design which is quick and easy. However, it requires a large number of samples to explore the design space, and re-sampling is required when the sample data cannot meet the expected requirements. On the other hand, the adaptive sampling approach uses the experimental design to obtain a certain number of initial sample points and followed by the determination of the next sample point according to the information obtained from the initial sample points and relevant evaluation criteria [19]. Compared with the one-time sampling approach, the adaptive sampling approach has better flexibility and high efficiency. In addition, the latter approach can effectively avoid over-sampling. Therefore, scholars over the world have conducted a large number of studies on how to obtain the next sampling point of the information about the last iteration. Xiong *et al.* [20] have formulated the adaptive sampling as an optimization problem. This approach combined the maximum and minimum distance with the projection distance, and the next sample point was obtained by algorithm optimization. Liu *et al.* [19] have used Monte Carlo approach and space reduction strategy combined with local boundary search algorithm to achieve adaptive sampling. However, the determination of sample points is independent of the output characteristics in these approaches. To improve the overall model accuracy efficiently, an adaptive sampling approach should utilize the characteristics of both inputs and outputs for choosing sample points. Jiang *et al.* [21] have proposed an adaptive sampling approach based on technique for order preference by similarity to an ideal solution (TOPSIS) and Delaunay triangulation, which achieved a balance between global exploration and local exploitation during the sampling process. Yang and Xue [22] have proposed a weighted adaptive sampling approach that comprehensively considered the influence of sample quality of the input and output parameter space. Jin *et al.* [23] have introduced the mean squared error (MSE) method for global meta-modeling. In this approach, the new sample point x_C with the largest mean squared error is selected form the existing Kriging model (created based on the existing sample set P_C) to complete the adaptive sampling. However, this technique is no longer applicable when meta-modeling techniques other than Kriging are used. Most of the current adaptive sampling techniques are only applicable to single-response problems. In addition, most of the engineering optimization problems are multi-response system problems. So, it has certain limitations. At the same time, there are limited studies on the optimization efficiency and application value of the combination of hybrid surrogate model and adaptive sampling approach.

In this article, a multi-response weighted adaptive sampling (MWAS) approach based on the hybrid surrogate model is proposed. This approach comprehensively considers the dispersion of sample points in the input design space and the fitting uncertainty of output response. Hence, the balance of global and local accuracy optimization can be achieved. The WPV of the hybrid surrogate model is used to identify areas with large local errors and the MDA approach is used to acquire the dispersion of sample points in the design space. In the iterative process, the weight coefficients are adaptively selected according to the accuracy of the hybrid surrogate model. Using this approach for sampling the design space, the sampling efficiency and the fitting accuracy of the surrogate model can be improved effectively.

II. THEORY OF MODEL OPTIMIZATION

A. HYBRID SURROGATE MODEL

Hybrid surrogate model was constructed by using weighted linear combinations of different surrogate models, and it is one of the best ways to improve the model prediction accuracy [24]. Its basic form is defined as:

$$\begin{cases} \hat{y}_{HS} = \sum_{i=1}^{N} w_i \hat{y}_i(x) \\ \sum_{i=1}^{N} w_i = 1 \end{cases} \tag{1}$$

where $\hat{y}_{HS}$ is the predicted response by the hybrid surrogate model, w_i, $\hat{y}_i$ are the weight and predicted response of ith sub-model respectively, N is the number of sub-models in the hybrid surrogate model.

In the hybrid surrogate model, the size of the weight coefficient reflects the predictive ability of the sub-model, and the more accurate sub-model should be assigned a larger weight coefficient. The root mean square error (RMSE) heuristic weighting scheme based on cross-validation was adopted to construct a hybrid surrogate model [25]. The formula is shown in Equation (2):

$$\begin{cases} w_i = \dfrac{w_i^*}{\sum_{j=1}^{N} w_j^*}, \quad w_i^* = (E_i + \alpha \bar{E})^{\beta} \\ \bar{E} = \dfrac{1}{N} \sum_{i=1}^{N} E_i, \quad E_i = RMSE_i = \sqrt{\dfrac{1}{M} \sum_{j=1}^{M} (y^j - \hat{y}^j)^2} \end{cases} \tag{2}$$

where y^j is the response of jth sample, $\hat{y}^j$ is the predicted response obtained for the surrogate model constructed using all sample points except the jth sample, E_i is the RMSE of ith sub-model, M is the number of sample, α and β

is respectively controlling the importance of averaging and sub-models, with values of 0.05 and −1.

The fitting accuracy of the surrogate model directly affects the feasibility and rationality of the optimal solution. Only if the surrogate model meets the accuracy requirements then the optimized solution has credibility. In order to assess the fitting accuracy of the surrogate model, two frequently used evaluation indicators were adopted: relative root mean square error (RRMSE) and relative maximum absolute error (RMAE) [26], [27]. The mathematical definitions of the two indicators are shown in Equation (3):

$$\begin{cases} \text{RRMSE} = \dfrac{\sqrt{\frac{1}{n_t}\sum_{i=1}^{n_t}(y_i - \hat{y}_i)^2}}{std} \\ \text{RMAE} = \dfrac{\text{Max}\left[y_i - \hat{y}_i\right]}{std} \end{cases} \tag{3}$$

where y_i and $\hat{y}_i$ are the actual response and the predicted response of ith test sample points respectively, n_t is the number of test sample points, and std is the standard deviation of y_i.

RRMSE represents the global accuracy of the surrogate model. The closer the value of RRMSE is to 0, the higher the global accuracy of the model. On the flip side, RMAE reflects the local accuracy of the surrogate model. The smaller the value of RMAE indicates the higher regional accuracy of the surrogate model.

According to research by Pan [28], when the hybrid surrogate model contains 3 to 5 sub-models, the prediction accuracy was the highest. Therefore, this paper constructs 9 single surrogate models (as shown in Table 1) based on different parameter settings, including 3 PRS models, 4 KRG models, 1 RBF model, and 1 EBF model. Then they were sorted according to the GMSE, and the three single surrogate models with the highest fitting accuracy were weighted to construct a hybrid surrogate model.

B. EXPERIMENTAL DESIGN

The selection of the preliminary sample points is the premise and foundation of the surrogate model construction. Mainstream experimental designs include optimal Latin hypercube design (OLHD), full factorial design, central composite design, and orthogonal array [29]–[33]. The OLHD is an experimental design approach proposed by Mckay *et al.* [29] to decrease the number of actual engineering simulation analysis experiments. This approach maximizes the stratification of each edge distribution to ensure full coverage of each variable range and then performs efficient sampling from the patchy distribution interval, which has very good space-filling and balance. Therefore, this paper adopts the OLHD to obtain the initial sample points. In the OLHD approach, the number of sampling points is usually selected according to the design variables and design space, and the number should not be less than the expected minimum sample point of the fitting surrogate model, as shown in Equation (4) [34].

$$N_C \geq 5n_s \tag{4}$$

where N_C is the number of sample points, n_s is the dimension of the design space.

III. MULTI-RESPONSE WEIGHTED ADAPTIVE SAMPLING (MWAS) APPROACH

In the proposed approach, the accuracy of the surrogate model is improved by considering the sample discreteness index in the input design space and the fitting uncertainty index of output response. In the iterative process, according to the influence of new sample points on the accuracy of the surrogate model, the weight coefficients of the two indices were determined to achieve the balance between global and local accuracy.

A. CALCULATION OF THE FITTING UNCERTAINTY INDEX OF OUTPUT RESPONSE BASED ON WEIGHTED PREDICTION VARIANCE

A strategy based on the prediction variance was used to calculate the deviation of the sub-model and the hybrid surrogate model at an unknown point in the input design space. This approach needs several different surrogate models to predict the response of candidate point x, and select the point with the largest divergence as the update point. The degree of divergence at point x is usually identified as the prediction variance of hybrid surrogate model [35]. The expression is shown in Equation (5):

$$\begin{cases} \sigma_{PV}^2(x) = \dfrac{1}{N}\sum_{i=1}^{N}(y_i(x) - \bar{y}(x))^2 \\ \bar{y}(x) = \dfrac{\sum_{i=1}^{N} y_i(x)}{N} \end{cases} \tag{5}$$

where y_i is the predicted value of ith sub-model, $\bar{y}$ is the average of the predicted value of N sub-models.

As can be recognized from Equation (5), the greater the predictive variance, the greater the difference between a sub-model and the hybrid surrogate model at that point. It indicated a great local error in the region. However, when the difference of the predicted value between a sub-model and the hybrid surrogate model is too obvious, the weight coefficient of the sub-model is too small. It is unreasonable for the next sample point completely determined by the sub-model. Meanwhile, the engineering optimization design problem is mostly a multi-response system, but the above-mentioned research is only applicable to the single response output. Combining the prediction variance strategy with the weight coefficient of the sub-model, a weighted prediction variance is proposed and used as a fitting uncertainty index.

The weighted prediction variance firstly uses a hybrid surrogate model constructed by N different sub-models to fit the multi-response system problem, and predicts all the

TABLE 1. Basic information of several sub-models.

ID	Sub-model	Details
1	PRS2	Full model of degree 2, 3 and 4 for Polynomial Response Surface
2	PRS3	
3	PRS4	
4	KRG-Gaussian	Four different Kriging models are selected by correlation models
5	KRG-Exponential	
6	KRG-Matern Linear	
7	KRG-Matern Cubic	
8	RBF	A type of neural network employing a hidden layer of radial units and an output layer of linear units
9	EBF	Similar to RBF but use elliptical units in place of radial units

responses of the candidate point x. The expression is shown in Equation (6):

$$\begin{cases} y_1 = \sum_{i=1}^{N} \omega_i f_{1i}(\mathrm{X}) \\ y_2 = \sum_{i=1}^{N} \omega_i f_{2i}(\mathrm{X}) \\ \quad \vdots \\ y_t = \sum_{i=1}^{N} \omega_i f_{ti}(\mathrm{X}) \end{cases} \tag{6}$$

where ω_i is the weight coefficient of the ith sub-model, t is the number of responses.

On the basis of Equation (5), the weighted predictive variance (WPV) expression was established by combining the weighted coefficients of the sub-model:

$$\begin{cases} \sigma^2_{WPV_j}(x) = \sum_{i=1}^{N} \omega_{ji} \left[y_{ji}(x) - y_{HS_j}(x) \right]^2 \\ 1 \le j \le t; \quad 1 \le i \le N \end{cases} \tag{7}$$

where ω_{ji} is the weight coefficient of jth sub-model in ith response.

For multi-response system problems, different responses may produce an order of magnitude difference in weighted prediction variance, so the weighted prediction variance of each response was normalized:

$$\begin{cases} \bar{\sigma}^2_{WPV_j}(x) = \dfrac{\sigma^2_{WPV_j}(x) - \min \sigma^2_{WPV_j}(x)}{\max \sigma^2_{WPV_j}(x) - \min \sigma^2_{WPV_j}(x)} \\ 1 \le j \le t \end{cases} \tag{8}$$

where $\sigma^2_{WPV_j}$ is the weighted prediction variance of jth response, $\bar{\sigma}^2_{WPV_j}$ is the normalized value of $\sigma^2_{WPV_j}$, $\max \sigma^2_{WPV_j}$ and $\min \sigma^2_{WPV_j}$ are the maximum and minimum WPV of jth response, respectively.

Finally, a multi-response weighted predictive variance expression was established by combining the correlation degrees of each response:

$$\sigma^2_{WPV}(x) = \sum_{i=1}^{t} \omega_j \bar{\sigma}^2_{WPV_j}(x) \tag{9}$$

where ω_j is the weight coefficient of jth response which is obtained by the entropy weight approach based on the initial sample data [36]. When $t = 1$, it is the single response version of the weighted prediction variance.

A one-dimensional test function was used to illustrate that the weighed prediction variance can efficiently identify the areas with large prediction deviations.

$$y = 2x^2 - 5x - 2(2\cos \pi x - 3 \sin \pi x) + 10 \tag{10}$$

The 9 surrogate models in Table 1 were constructed from 7 sample points uniformly distributed in the design space. Figure 1(a) show the difference between the predicted curve of the hybrid surrogate model and the actual function curve. It can be seen from the figure that the weighted prediction variance has a good correlation with the actual error. The location of the new sample point is the region with the largest actual deviation. Figure 1(b) show the comparison between the weighted prediction variance and the actual deviation square. The results showed that weighted prediction variance and the actual deviation have the same increase and decrease trend. The positions of the maximum points of the weighted prediction variance curve and the actual deviation curve are consistent. It indicated that this approach can effectively identify the area with large local error.

From the above research, it can be concluded that fitting uncertainty index can effectively identify areas with large local error. However, this approach only considers the output response. Furthermore, in the absence of constraints, update points tend to cluster in a small area. When points are clustered together, the matrix used to fit the surrogate model will have ill-conditioned mutations, which will lead to a poor fit.

B. CALCULATION OF THE SAMPLE DISCRETENESS INDEX IN THE INPUT DESIGN SPACE BASED ON MAXIMUM AND MINIMUM DISTANCE APPROACH

To solve the problem that poor fitting of the surrogate model caused by sample point aggregation, and to make the sample distribution sparse in areas with insensitive fitting accuracy, a distance term d was added to make the trade-off between uniformity and sparseness of samples in different regions. However, it is difficult to determine a suitable distance term d in practical applications. When d is too large, the sample points in the area with large local error will be filtered out, and the area with heavy local error cannot be effectively explored.

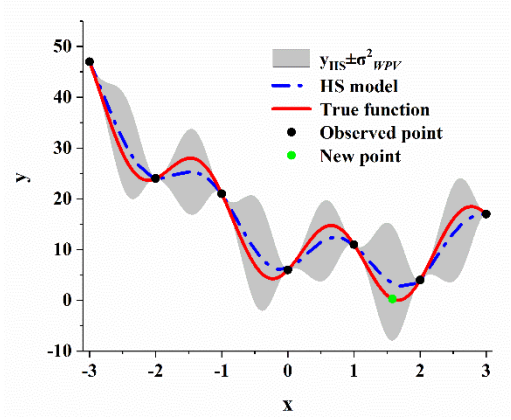

(a) Difference of predicted curve and actual function curve.

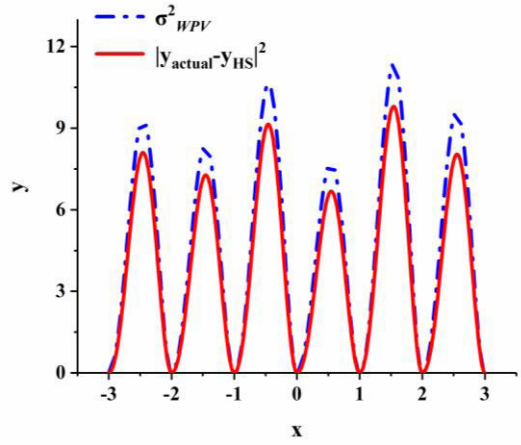

(b) Comparison of WPV and actual error square.

FIGURE 1. A one-dimensional example to show the WPV.

When d is too low, the phenomenon of clustering of sample points cannot be avoided. Based on Euclidean distance, the maximum and minimum distance approach maximizes the minimum distance between the next sampling point and all sample points in the design space, which can effectively filter the collected samples and provide a good sample uniform distribution [37]. Therefore, the MDA was selected to account for the distance item d and used as a sample discreteness index. Its expression is shown in Equation (11):

$$\begin{cases} \max\limits_{P_K}[\min\limits_{1\le i\le k, c\le j\le c+k}^{P_{Ki}\ne P_{Aj}}(d(\mathrm{x}_{Ki},\mathrm{x}_{Aj}))] \\ d(\mathrm{x}_i,\mathrm{x}_j)=\min\limits_{\mathrm{x}_i,\mathrm{x}_j\in P}\sqrt{\sum_{u=1}^{m}\left|x_i^u-x_j^u\right|^2} \\ P=(\mathrm{x}_1,\mathrm{x}_2,\ldots,\mathrm{x}_n),\ \mathrm{x}_i=\left(x_i^1,x_i^2,\ldots,x_i^m\right) \end{cases} \tag{11}$$

where n and m are the number of sample points and design variables respectively, $P_{Aj}\in P_A=P_C\cup P_K$, P_A is the total sample set, P_K is a new sample set, P_C is the initial sample set, P_{Aj} is the jth sample point in P_A, P_{Ki} is the ith sample point in P_K, k is the number of new sample points, c is the number of initial sample points.

C. PRINCIPLE OF THE MULTI-RESPONSE WEIGHTED ADAPTIVE SAMPLING APPROACH

In the multi-response weighted adaptive sampling approach, the selection of the next sample point is mainly determined by the two indices (fitting uncertainty and sample discreteness) and the weight coefficients considering importance of these indices. As shown in Equation (12):

$$\begin{cases} \max f(\mathrm{x}_{n+1})=\max(\omega_1 f_d(\mathrm{x}_{n+1})+\omega_2 f_v(\mathrm{x}_{n+1})) \\ \omega_1+\omega_2=1 \end{cases} \tag{12}$$

where $f_d(\mathrm{x}_{n+1})$ and $f_v(\mathrm{x}_{n+1})$ are sample discreteness index and fitting uncertainty index respectively, ω_1 and ω_2 are the weight coefficients of $f_d(\mathrm{x}_{n+1})$ and $f_v(\mathrm{x}_{n+1})$ respectively.

The sample discreteness index and fitting uncertainty index were normalized to avoid misleading the acquisition of new sampling points caused by the difference in orders of magnitude.

$$\begin{cases} f_d(\mathrm{x}_{n+1})=\dfrac{d_{\min}(\mathrm{x}_{n+1},\mathrm{x}_{Aj})-\min d_{\min}(\mathrm{x}_{n+1},\mathrm{x}_{Aj})}{\max d_{\min}(\mathrm{x}_{n+1},\mathrm{x}_{Aj})-\min d_{\min}(\mathrm{x}_{n+1},\mathrm{x}_{Aj})} \\ f_v(\mathrm{x}_{n+1})=\dfrac{\sigma^2_{WPV_j}(\mathrm{x}_{n+1})-\min\sigma^2_{WPV_j}(\mathrm{x}_{n+1})}{\max\sigma^2_{WPV_j}(\mathrm{x}_{n+1})-\min\sigma^2_{WPV_j}(\mathrm{x}_{n+1})} \end{cases} \tag{13}$$

In the adaptive sampling process, the global accuracy was gradually improved with the increasing of sample points, and it was more reliable when looking for the next sample point. Therefore, ω_1 is a large number in the early stage of adaptive sampling, and ω_2 takes a larger value in the later stage. The values of ω_1 and ω_2 are determined by Equation (14) and Equation (15):

$$\begin{cases} \omega_1=(0.7,0.9],R^2\in(0,0.6] \\ \omega_1=(0.5,0.7],R^2\in(0.6,0.8] \\ \omega_1=(0.2,0.5],R^2\in(0.8,1.0) \\ \omega_2=1-\omega_1 \end{cases} \tag{14}$$

$$\mathrm{R}^2=1-\frac{\sum_{i=1}^{n_t}(y_i-\hat{y}_i)^2}{\sum_{i=1}^{n_t}(y_i-\bar{y}_i)^2} \tag{15}$$

where $\bar{y}_i$ is the average value of the actual response value, n_t is the number of test sample points. R^2 reflects the global accuracy of the surrogate model. The closer the value of R^2 is to 1, the higher the global accuracy of the model [31].

D. PROCESS OF MULTI-RESPONSE WEIGHTED ADAPTIVE SAMPLING APPROACH

Figure 2 displays a flowchart of the MWAS approach. Firstly, the initial sample set P_C with n sample points was generated by OLHD, and the responses of all sample points were achieved by simulation analysis or experiment. Secondly, the initial sample set P_C was used to construct the 9 surrogate models in Table 1, and the hybrid surrogate model was

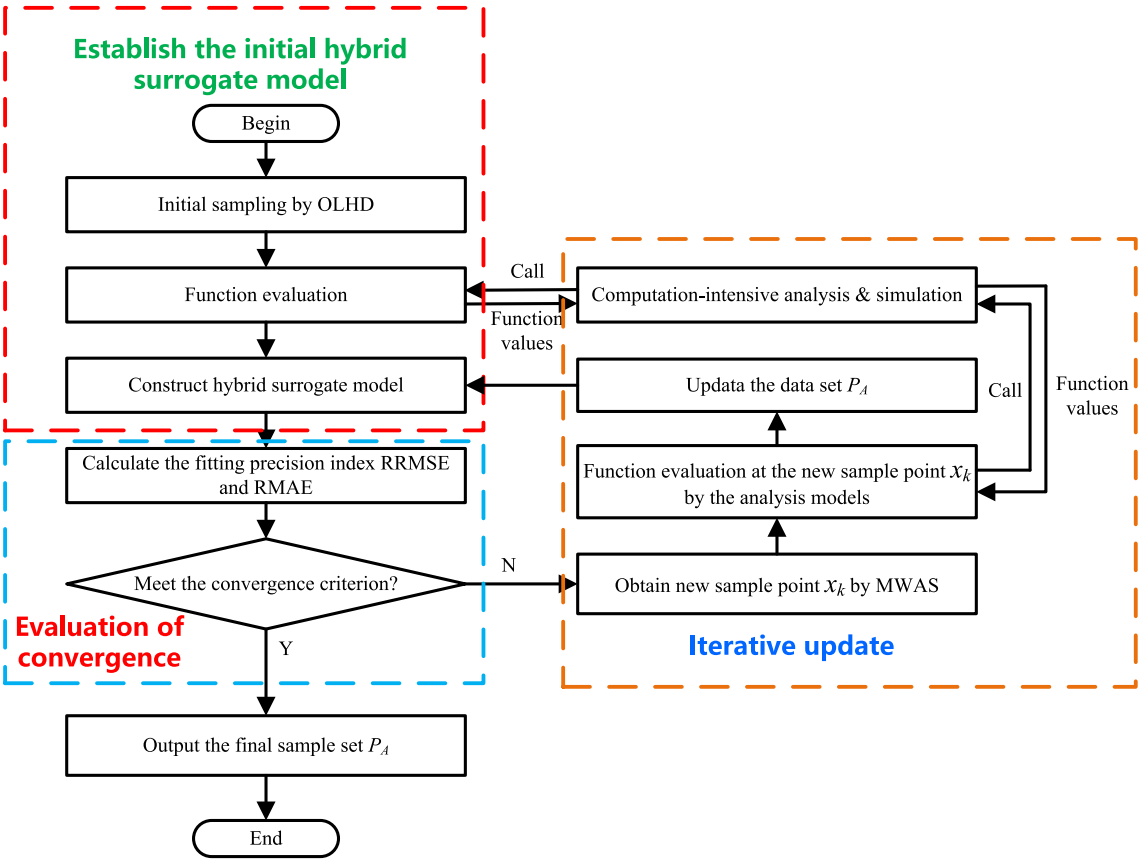

FIGURE 2. Flowchart of the MWAS approach.

constructed by using three sub-models with the highest accuracy. Then, the two indices (fitting uncertainty and sample discreteness) of the candidate sample points were calculated, and the next update point was determined by solving the optimization problem in Equation (12). Import the update point into the simulation model to obtain the sample response value of kth iteration. Finally, the hybrid surrogate model was reconstructed by using the total sample set P_A, and the fitting accuracy evaluation index (RRMSE, RMAE) was calculated depending on Equation (3). If surrogate model accuracy meets the convergence criteria or computed resources (budget or time) are exhausted. No additional samples are needed and the final sample set of P_A is the output. Otherwise, continue to cycle sampling to obtain a new sample point.

IV. NUMERICAL EXAMPLE

A. TEST FUNCTION

In order to evaluate the practical feasibility of the MWAS. Three test functions were applied to form three single-response and four multi-response systems for test analysis. The three test functions are shown in Equation (16-18). Figure 3 shows the basic shapes of the three test functions.

$$\begin{aligned} \text{F1}: f_1(x_1, x_2) &= (x_1^2 + x_2 - 11)^2 + (x_2^2 + x_1 - 7)^2, \\ x_1, x_2 &\in [-3, 3] \end{aligned} \tag{16}$$

$$\begin{aligned} \text{F2}: f_2(x_1, x_2) &= 2x_1^2 - 1.05x_1^4 + \frac{x_1^6}{6} + x_1x_2 + x_2^2, \\ x_1, x_2 &\in [-3, 3] \end{aligned} \tag{17}$$

$$\begin{aligned} \text{F3}: f_3(x_1, x_2) &= 3(1 - x_1)^2 \exp(-x_1^2 - (x_2 + 1)^2) \\ &\quad - 10(\frac{x_1}{5} - x_1^3 - x_2^5) \exp(-x_1^2 - x_2^2) \\ &\quad - \frac{1}{3} \exp(-(x_1 + 1)^2 - x_2^2), \\ x_1, x_2 &\in [-3, 3] \end{aligned} \tag{18}$$

B. TEST SCHEME

For comparison, the other four approaches were adopted to test the examples, including the MSE [23], MDA, WPV and OLHD. For the four adaptive sampling approaches, 10 initial sample points were generated by OLHD, and 25 sample points were gradually collected through their respective adaptive sampling principles. While OLHD collected 35 sample points at one-time. Accuracy evaluation indices RRMSE and RMAE of the surrogate model were calculated based on 1000 test sample points obtained by OLHD. Global and local accuracy (RRMSE and RMAE) of the surrogate model constructed with the same total sample size was used to measure the sampling efficiency. The smaller the RRMSE and RMAE under the equal sample size, the better the sampling efficiency.

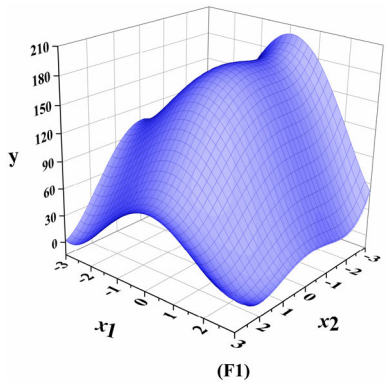

(a) Obtained by Equation (16).

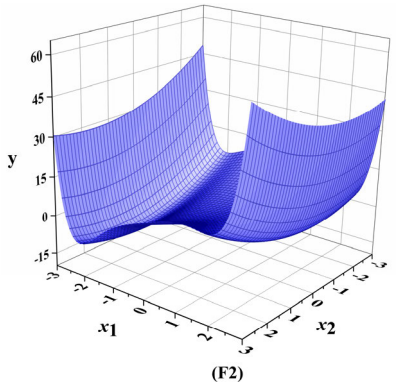

(b) Obtained by Equation (17).

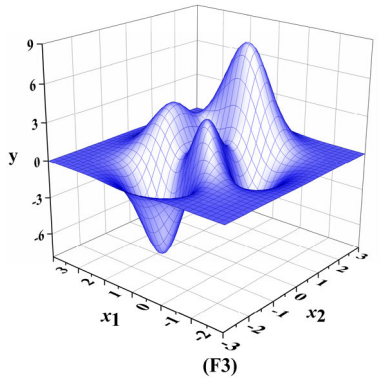

(c) Obtained by Equation (18).

FIGURE 3. The plots of test functions.

C. COMPARISON AND ANALYSIS

The proposed single response version of MWAS was applied to three single response functions for analysis. Accuracy results of different sampling methods are listed in Table 2, and the best results are indicated in bold.

It can be seen from Table 2 that when the sample size was the same, the global and local accuracy obtained by the MWAS approach was higher than the other four sampling methods. Compared with the WPV and MDA approaches, the MWAS approach (which comprehensively considers the fitting uncertainty of output response and the sample dispersion) has higher sampling efficiency. At the same time, the local accuracy of the surrogate model constructed

TABLE 2. The accuracy results of single-response systems by different sampling methods.

Single response system	Accuracy criteria	MWAS	WPV	MDA	MSE	OLHD
F1	RRMSE	**0.027**	0.040	0.056	0.084	0.061
	RMAE	**0.106**	0.136	0.483	0.498	0.632
F2	RRMSE	**0.059**	0.111	0.189	0.156	0.093
	RMAE	**0.308**	0.353	0.648	0.439	0.767
F3	RRMSE	**0.160**	0.326	0.851	0.362	0.320
	RMAE	**0.503**	1.500	3.049	1.520	1.552

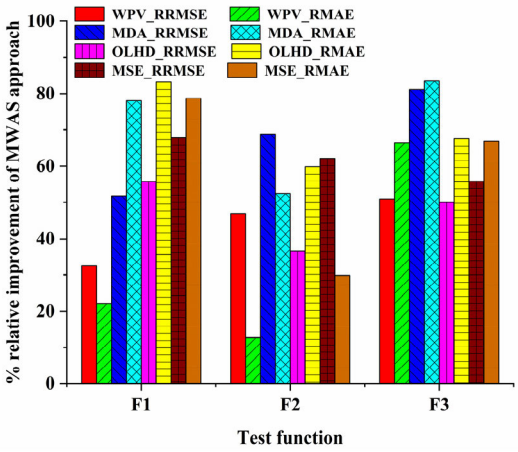

FIGURE 4. The improvement in RRMSE and RMAE for MWAS relative to the other four sampling approaches.

by WPV is better than that of MDA, MSE and OLHD approaches.

Comparing MWAS with the other four sampling methods, improvements of RRMSE and RMAE are shown in Figure 4. MWAS method significantly improved the accuracy of the surrogate model compared to the other four sampling approaches, and was more prominent in the test function F3, which changed dramatically in response.

To compare the performance of the proposed MWAS on multi-response system problems, five sampling methods were applied to four multi-response systems. Table 3 shows the model accuracy of five multi-response system problems. The bottom of the table shows the average and standard deviation of the three test functions for the accuracy of the surrogate model in the different multi-response system. In Table 3, the best results are indicated in bold.

Table 3 shows that under the same number of samples, MWAS method achieved the best model accuracy, followed by WPV. From the results of the standard deviation, it can be concluded that MWAS approach has better robustness in the F1 and F3 functions, while it performs worse than the other approach in the F2 function. Meanwhile, the proposed MWAS approach can provide a more accurate surrogate

TABLE 3. The accuracy results of multi-response systems by different sampling methods.

Multi-response systems	Test functions	Accuracy criteria	MWAS	WPV	MDA	MSE	OLHD
F1+F2	F1	RRMSE	0.088	0.187	**0.079**	0.116	0.092
		RMAE	**0.234**	0.845	0.541	0.629	0.723
	F2	RRMSE	**0.074**	0.182	0.235	0.155	0.170
		RMAE	**0.319**	0.644	1.071	0.596	1.082
F1+F3	F1	RRMSE	0.071	**0.042**	0.054	0.079	0.068
		RMAE	0.324	**0.200**	0.308	0.400	0.707
	F3	RRMSE	**0.301**	0.309	0.426	0.371	0.390
		RMAE	**1.030**	1.049	1.986	1.269	1.539
F2+F3	F2	RRMSE	0.141	**0.099**	0.154	0.212	0.141
		RMAE	0.699	**0.562**	1.134	0.734	1.071
	F3	RRMSE	**0.280**	0.335	0.446	0.326	0.445
		RMAE	**0.894**	1.198	2.034	1.194	2.029
F1+F2+F3	F1	RRMSE	**0.066**	0.099	0.074	0.088	0.085
		RMAE	**0.204**	0.446	0.301	0.339	0.503
	F2	RRMSE	0.223	0.181	0.176	0.272	**0.154**
		RMAE	0.815	**0.672**	0.776	0.838	1.308
	F3	RRMSE	**0.284**	0.408	0.500	0.458	0.442
		RMAE	**1.269**	1.506	2.280	1.696	2.040
AVE	F1	RRMSE	0.075	0.109	**0.069**	0.094	0.082
		RMAE	**0.254**	0.497	0.383	0.456	0.644
	F2	RRMSE	**0.146**	0.154	0.188	0.213	0.155
		RMAE	**0.611**	0.626	0.994	0.723	1.154
	F3	RRMSE	**0.288**	0.351	0.457	0.385	0.426
		RMAE	**1.064**	1.251	2.100	1.386	1.869
SD	F1	RRMSE	**0.009**	0.06	0.011	0.016	0.010
		RMAE	**0.051**	0.266	0.112	0.125	0.100
	F2	RRMSE	0.061	0.039	0.034	0.048	**0.012**
		RMAE	0.212	**0.047**	0.156	0.099	0.109
	F3	RRMSE	**0.009**	0.042	0.031	0.055	0.025
		RMAE	0.155	0.190	**0.129**	0.221	0.234

model for multi-response system problems with different characteristics. At the same sample size, the model accuracy of the test function in the multi-response system was lower than that in the single-response system because as the size of the system increased, the effect of output responses with more different characteristics on sample update point location selection needs to be considered.

V. LIGHTWEIGHT DESIGN OF PASSENGER CAR REAR SEAT

A. LUGGAGE COLLISION TEST OF PASSENGER CAR REAR SEAT

Figure 5 shows the principle of a luggage collision test of passenger car rear seat. According to the requirements of GB15083-2006, a passenger car rear seat assembly and two test specimens with a size of 300 mm × 300 mm × 300 mm, edge chamfer of 20 mm and mass of 18 kg were placed in the trolley test bench. Then, the acceleration-time curve illustrated in Figure 5(a) was applied to the trolley test bench to simulate a passenger car collision. Figure 5(b) shows the state of the passenger car's rear seat at a certain moment during the collision [38]. The finite element model of the luggage collision test was established by HyperMesh software and solved by using Ls_Dyna software (as shown in Figure 5(c)).

B. SELECTION OF DESIGN VARIABLES AND RESPONSES

During the luggage collision test, the main force and energy-absorbing component was the backrest skeleton. Therefore, according to the symmetry and functionality of the backrest skeleton structure, the tube and plate parts of the backrest skeleton were simplified into 5 sets of optimized parts (as showed in Figure 6) marked as P_1 to P_5. The thickness

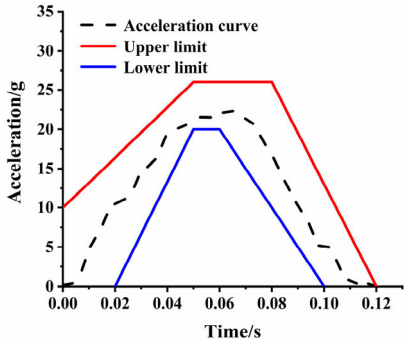

(a) Seat dynamic test loading curve.

(b) Luggage collision real object test.

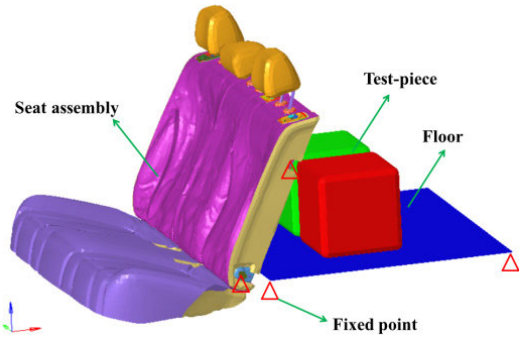

(c) Finite element model of luggage collision test.

FIGURE 5. Analysis diagram of passenger car rear seat luggage collision test.

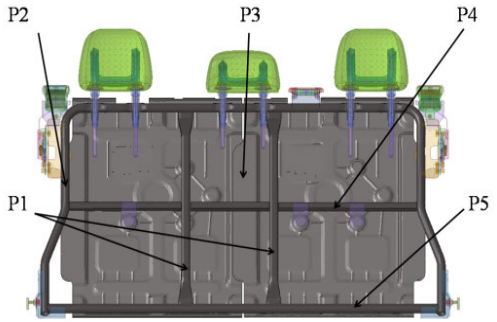

FIGURE 6. Distribution of optimized parts.

TABLE 4. Candidate materials for lightweight design.

Material no	Material name	SIGY (MPa)	UTS (MPa)	PE (%)	Relative cost
101	DC04	165	372.6	0.322	1.21
102	DC01	172	451.4	0.358	1.00
103	SAPH370	225	492.1	0.285	1.10
104	SAPH400	255	528	0.278	1.15
201	Q235_TUBE	300	639.8	0.354	1.09
202	SAPH440	374.75	653.7	0.308	1.11
203	Q345_TUBE	455.5	625.8	0.251	1.22
204	QSTE420TM	459.7	691.6	0.253	1.32
301	B410LA	530	759	0.278	1.30
302	S650MC	650	814	0.095	1.36
303	HC700LA	700	899.25	0.086	1.45
304	20CrMnTi	835	1188	0.095	1.56

TABLE 5. Range of design variables for lightweight design.

Thickness variables	Origin value/ mm	Optional values/ mm	Material variables	Range
t_1	1.5	1.0，1.1，…，1.8	m_1	301-304
t_2	1.5	1.0，1.1，…，1.8	m_2	201-204
t_3	1.2	0.8，0.9，…，1.6	m_3	101-104
t_4	1.2	0.8，0.9，…，1.6	m_4	201-204
t_5	1.8	1.4，1.5，…，2.2	m_5	201-204

and material of the optimized parts are invoked as design variables, which were marked as t_1-t_5 and m_1-m_5 respectively.

Table 4 shows the main performance parameters of candidate materials for optimized parts, including yield strength (SIGY), ultimate tensile strength (UTS), percentage elongation (PE), and relative cost. The candidate materials are divided into three groups concerning a gradual increasing value of SIGY. Table 5 exhibited the value ranges of the design variables.

According to regulation, the front profile of the headrests is not allowed to be moved out of the 150 mm horizontal-vertical plane in front of the seat design reference point during the test. The backrest skeleton and its fasteners are permitted to have a certain degree of deformation, provided that they can't fail. The maximum strain criterion was adopted as the failure criterion, and introduced the strain index (as shown in Equation (19)) to judge whether the component fails. When the strain index is greater than 1, it means that the component is in a failure state; otherwise, it is in a safe state [39]. Therefore, the maximum displacement of the headrest (L), the strain index of each optimized parts (Q_i), the total mass (M) and total price (C) of the optimized parts are used as evaluation indicators for safety performance and lightweight.

$$Q_i = \frac{S_i}{E_i} \tag{19}$$

where Q_i represents the strain index of ith component, S_i is the maximum plastic strain of ith component, E_i is the elongation of the material used in ith component.

TABLE 6. Accuracy evaluation results of each response.

Responses	Accuracy criteria	MWAS	WPV	MDA	MSE
M	RRMSE	**0.017**	0.023	0.033	0.034
	RMAE	**0.045**	0.058	0.114	0.070
C	RRMSE	0.105	0.106	0.153	**0.104**
	RMAE	0.280	0.228	0.403	**0.213**
L	RRMSE	**0.116**	0.122	0.117	0.121
	RMAE	**0.258**	**0.258**	0.286	0.261
Q_1	RRMSE	**0.438**	0.514	0.584	0.481
	RMAE	**1.253**	1.314	1.388	1.367
Q_2	RRMSE	**0.329**	0.386	0.411	0.361
	RMAE	**0.649**	0.895	1.184	0.930
Q_3	RRMSE	**0.332**	0.366	0.348	0.412
	RMAE	**0.829**	0.970	0.925	0.864
Q_4	RRMSE	**0.349**	0.536	0.492	0.508
	RMAE	**1.126**	1.703	1.387	1.288
Q_5	RRMSE	**0.235**	0.292	0.315	0.312
	RMAE	**0.720**	0.753	0.819	0.729
AVE	RRMSE	**0.240**	0.293	0.307	0.292
	RMAE	**0.645**	0.772	0.813	0.715

In summary, this 10-dimensional multi-response system problem with 8 output responses can be expressed as:

$$\begin{cases} M(t,m), C(t,m), L(t,m), \\ Q_i(t,m), i = [1,2,\ldots,5], \\ t = [1.0, 1.1, \ldots, 2.2], \\ m = [101, 102, 103, 104, 201, 202, \\ \quad 203, 204, 301, 302, 303, 304] \end{cases} \tag{20}$$

where $M(t,m)$ and $C(t,m)$ are the total mass and total price of optimized parts respectively, $L(t,m)$ is the maximum displacement of the headrest, $Q_i(t,m)$ is the strain index of ith optimized part, t is the thickness design variable, m is the material design variable.

C. ADAPTIVE SAMPLING SCHEME

Considering that the high-fidelity collision simulation is a very time consuming work. In this section, only four adaptive sampling approaches were used for comparison. Firstly, the OLHD method was used to obtain 100 initial sample points and 2000 candidate sample points respectively. Then, four adaptive sampling approaches were used to iteratively add 60 new sample points from the candidate sample points on the basis of the surrogate model constructed by the initial sample points. Finally, 50 random sample points were used to estimate the accuracy of each surrogate model to judge the sampling efficiency of the four adaptive sampling approaches.

Table 6 shows the model accuracy of each response in the lightweight design of passenger car rear seats, and the best results are indicated in bold. It can be seen from the table that, under the same number of sample points, the surrogate model accuracy obtained by MWAS method was the best except for response C. Among them, the three lower nonlinear responses of M, C, and L have lower requirements on the number of samples. With a large number of sample points, the four methods all achieved high accuracy, among which MWAS and MSE performed better. Compared with the other three adaptive sampling methods, MWAS has a great improvement in global and local accuracy for five high nonlinear responses from Q_1 to Q_5. It shows that the MWAS method has useful application value for complex engineering optimization problems.

TABLE 7. Parameters of NSGA-II.

Parameter	Value
Population Size	100
Number of Generations	120
Crossover Probability	0.9
Crossover Distribution Index	10
Mutation Distribution Index	20
Max Failed Runs	5
Failed Run Penalty Value	1.0E30
Failed Run Objective Value	1.0E30

D. MULTI-OBJECTIVE OPTIMIZATION

The thickness and material types of the optimized parts were simultaneously taken as design variables and the strain index of the optimized parts were taken as constraints. Then, the total mass and price of the optimized parts, together with the maximum displacement of the headrest, were selected as three conflicting optimization objectives. The constraint value was set to be 0.8, after the error of simulation results and the safety factor of the product were taken into account. Therefore, the final multi-objective optimization design mathematical model of passenger car rear seat is shown in Equation (21):

$$\begin{cases} Minimize \ \{M(t,m), C(t,m), L(t,m)\}, \\ S.t. \ \ Q_i(t,m) \le 0.8, i = [1,2,\ldots 5], \\ t = [1.0, 1.1, \ldots, 2.2], \\ m = [101, 102, 103, 104, 201, 202, \\ \quad 203, 204, 301, 302, 303, 304] \end{cases} \tag{21}$$

NSGA-II algorithm was utilized to solve the multi-objective optimization problem of Equation (21) based on the hybrid surrogate model [40]. The parameter setting of NSGA-II algorithm was presented in Table 7. Due to the reason that the optimization results obtained by NSGA-II algorithm were stochastic, 10 runs were performed and then the optimal solution set with the best Pareto frontier distribution were taken as the final choice. Finally, 106 Pareto optimal solutions were obtained after 12,000 evaluations. Figure 7 displays the distribution of Pareto solution set in the objective space. It could be seen from the figure that the distribution of Pareto solution set in the objective space is a continuous and narrow spatial surface. It shows that the

TABLE 8. Comparison of the original and optimum responses.

Type	M	L	C	Q1	Q2	Q3	Q4	Q5
Purposes	Min	Min	Min	≤0.8	≤0.8	≤0.8	≤0.8	≤0.8
Original	10.53	84.88	11.76	0.284	0.371	0.609	1.295	0.351
Post-Lightweight	7.42	86.70	8.29	0.433	0.762	0.594	0.657	0.269
Simulation	7.35	85.26	8.04	0.425	0.784	0.614	0.685	0.268
Error/%	2.97	1.66	0.90	1.90	2.91	3.45	4.20	0.43
Change/%	31.63	-0.45	30.20	-49.65	-111.32	-0.82	47.10	23.65

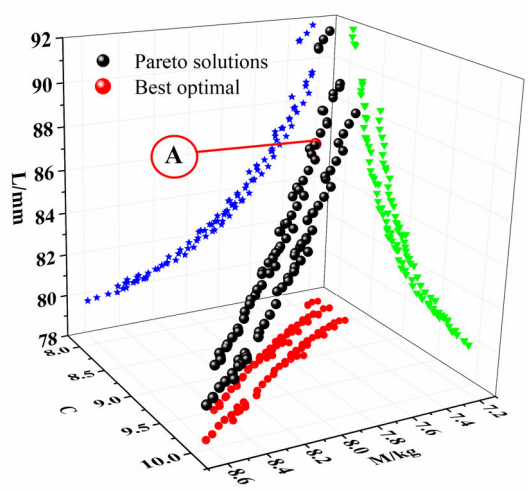

FIGURE 7. Distribution of Pareto solutions in the three-objective space.

comprehensive performance of the optimized result is fine, and there won't be a large number of optimal solutions with superior performance for a single objective. However, selecting a specific solution based on subjective consciousness and engineering experience has a certain degree of randomness. Therefore, this paper uses the TOPSIS method [41] to select the optimal compromise solution from the multi-objective optimization problem.

E. VERIFICATION OF LIGHTWEIGHT DESIGN

After obtaining the best compromise solution, it is very important to verify whether the optimized result is appropriate. Table 8 exhibits the comparison before and after the lightweight of the rear seat of passenger car. It can be seen from the table that the mass and relative cost of the optimized parts in the optimized solution are reduced from the original value of 10.53kg to 7.42kg, and 11.76 to 8.04 (i.e. the weight is reduced by 31.63% and the relative cost is reduced by 30.20%). At the same time, the displacement of the headrest has increased slightly, from the original value of 84.88 to 85.26 mm (i.e. an increased by 0.45%), but there is always a large margin from the 150 mm required by regulations. Compared with the original value, the strain index of the optimized parts has increased or decreased, but they are all within the range of the safety factor and meet the regulation requirements. Therefore, in lightweight design, it is more feasible to use the TOPSIS method to select the optimal compromise solution. The error between the optimized solution of each response and its simulation value were below 4.5%, indicated that the hybrid surrogate model based on the MWAS method has a better accuracy guarantee. One completed luggage crash simulation for a passenger car rear seat needs 6 to 8 hours. The computational cost of lightweight design of passenger car rear seats will be greatly reduced by adopting the proposed MWAS method based on the hybrid surrogate model.

VI. CONCLUSION

With the intention to improve the accuracy of the surrogate model and optimize efficiency, in this article a WPV approach based on the hybrid surrogate model was proposed to identify areas with large predicted deviations, and a MWAS approach was established by combining it with MDA.

(a) Through a one-dimensional test function, it is shown that the weighted prediction variance and the actual error have the same increase and decrease trend, and the maximum value was located in the same area, indicated that the approach can effectively identity areas with large local errors.

(b) Based on numerical examples and engineering cases, the sampling efficiency of MWAS, WPV, MDA, MSE and OLHD sampling methods were compared. All results showed that under the same number of sample points, MWAS has the highest accuracy of the surrogate model, that is, MWAS has the highest sampling efficiency. It indicated that MWAS can efficiently guide adaptive sampling and is useful for complex engineering optimization problems with long solution time and small maximum allowable sampling points.

(c) The MWAS method was applied to the rear seats of passenger cars for structure-material integration multi-objective lightweight design. The optimization solution obtained by NSGA-II algorithm optimization was compared with the pre-optimization scheme. Under the premise of ensuring that multiple performance indicators of the seat meet the requirements of regulations. The mass and cost of the optimized parts were reduced by 31.63% and 30.20%, respectively. Meanwhile, the headrest displacement increased by 0.45%. The error between the optimized solution of each response and its simulation value was below 4.5%. It can be seen that the hybrid surrogate model has an ideal fitting accuracy in the luggage collision simulation of passenger car rear seats.

REFERENCES

[1] N. Asadinia, A. Khalkhali, and M. J. Saranjam, "Sensitivity analysis and optimization for occupant safety in automotive frontal crash test," *Latin Amer. J. Solids Struct.*, vol. 15, no. 7, pp. 1–15, Jul. 2018.

[2] Y. Qin, X. Tang, T. Jia, Z. Duan, J. Zhang, Y. Li, and L. Zheng, "Noise and vibration suppression in hybrid electric vehicles: State of the art and challenges," *Renew. Sustain. Energy Rev.*, vol. 124, May 2020, Art. no. 109782.

[3] X. Tang, T. Jia, X. Hu, Y. Huang, Z. Deng, and H. Pu, "Naturalistic data-driven predictive energy management for plug-in hybrid electric vehicles," *IEEE Trans. Transport. Electrific.*, early access, Sep. 21, 2020, doi: 10.1109/TTE.2020.3025352.

[4] X. Hu, C. Zou, X. Tang, T. Liu, and L. Hu, "Cost-optimal energy management of hybrid electric vehicles using fuel cell/battery health-aware predictive control," *IEEE Trans. Power Electron.*, vol. 35, no. 1, pp. 382–392, Jan. 2020.

[5] Y. Wu, Q. Yin, H. Jie, B. Wang, and J. Zhao, "A RBF-based constrained global optimization algorithm for problems with computationally expensive objective and constraints," *Struct. Multidisciplinary Optim.*, vol. 58, no. 4, pp. 1633–1655, Apr. 2018.

[6] M. Lwin, J. Guo, N. Dimitrov, and S. Santoso, "Protective device and switch allocation for reliability optimization with distributed generators," *IEEE Trans. Sustain. Energy*, vol. 10, no. 1, pp. 449–458, Jan. 2019.

[7] D. Wang, R. Jiang, and Y. Wu, "A hybrid method of modified NSGA-II and TOPSIS for lightweight design of parameterized passenger car sub-frame," *J. Mech. Sci. Technol.*, vol. 30, no. 11, pp. 4909–4917, Nov. 2016.

[8] Y. Zhang, Z. Sun, Y. Yan, Z. Yu, and J. Wang, "An efficient adaptive reliability analysis method based on kriging and weighted average misclassification rate improvement," *IEEE Access*, vol. 7, pp. 94954–94965, 2019.

[9] J. Park and I. W. Sandberg, "Universal approximation using radial-basis-function networks," *Neural Comput.*, vol. 3, no. 2, pp. 246–257, Jun. 1991.

[10] J. Kleijnen, "Kriging meta-modeling in simulation: A review," *Eur. J. Oper. Res.*, vol. 192, no. 3, pp. 707–716, Feb. 2009.

[11] A. Shokri and M. Dehghan, "A meshless method using radial basis functions for the numerical solution of two-dimensional complex Ginzburg-Landau equation," *CMES Comput. Model. Eng. Sci.*, vol. 84, no. 4, pp. 333–358, Apr. 2012.

[12] S. Sajavičius, "Radial basis function method for a multidimensional linear elliptic equation with nonlocal boundary conditions," *Comput. Math. with Appl.*, vol. 67, no. 7, pp. 1407–1420, Apr. 2014.

[13] F. Xiong, D. Wang, Z. Ma, S. Chen, T. Lv, and F. Lu, "Structure-material integrated multi-objective lightweight design of the front end structure of automobile body," *Struct. Multidisciplinary Optim.*, vol. 57, no. 2, pp. 829–847, Feb. 2018.

[14] L. Zerpa, N. Queipo, and S. Pintos, "An optimization methodology of alkaline-surfactant-polymer flooding processes using field scale numerical simulation and multiple surrogates," *J. Petroleum Sci. Eng.*, vol. 47, pp. 197–208, Jun. 2005.

[15] L. Chen, H. Qiu, C. Jiang, X. Cai, and L. Gao, "Ensemble of surrogates with hybrid method using global and local measures for engineering design," *Struct. Multidisciplinary Optim.*, vol. 57, no. 4, pp. 1711–1729, Apr. 2018.

[16] J. Zhang, X. Yue, J. Qiu, M. Zhang, and X. Wang, "A unified ensemble of surrogates with global and local measures for global metamodelling," *Eng. Optim.*, vol. 53, no. 3, pp. 474–495, Mar. 2020.

[17] H. Yin, H. Fang, G. Wen, M. Gutowski, and Y. Xiao, "On the ensemble of metamodels with multiple regional optimized weight factors," *Struct. Multidisciplinary Optim.*, vol. 58, no. 1, pp. 245–263, Jul. 2018.

[18] Y. Liu, Y. Shi, Q. Zhou, and R. Xiu, "A sequential sampling strategy to improve the global fidelity of metamodels in multi-level system design," *Struct. Multidisciplinary Optim.*, vol. 53, no. 6, pp. 1295–1313, Jan. 2016.

[19] H. Liu, S. Xu, and X. Wang, "Sequential sampling designs based on space reduction," *Eng. Optimiz.*, vol. 47, no. 7, pp. 1–18, Jun. 2014.

[20] F. Xiong, Y. Xiong, W. Chen, and S. Yang, "Optimizing latin hypercube design for sequential sampling of computer experiments," *Eng. Optim.*, vol. 41, no. 8, pp. 793–810, Jul. 2009.

[21] P. Jiang, Y. Zhang, Q. Zhou, X. Shao, J. Hu, and L. Shu, "An adaptive sampling strategy for Kriging metamodel based on delaunay triangulation and TOPSIS," *Int. J. Speech Technol.*, vol. 48, no. 6, pp. 1644–1656, Aug. 2017.

[22] Q. Yang and D. Xue, "A weighted sequential sampling method considering influences of sample qualities in input and output parameter spaces for global optimization," *J. Optim. Theory Appl.*, vol. 164, no. 2, pp. 644–665, Feb. 2015.

[23] R. Jin, W. Chen, and A. Sudjianto, "On sequential sampling for global metamodeling in engineering design," in *Proc. 28th Design Autom. Conf.*, vol. 2, Jan. 2002, pp. 539–548.

[24] E. Acar, "Effect of error metrics on optimum weight factor selection for ensemble of metamodels," *Expert Syst. Appl.*, vol. 42, no. 5, pp. 2703–2709, Apr. 2015.

[25] M. Babaei and I. Pan, "Performance comparison of several response surface surrogate models and ensemble methods for water injection optimization under uncertainty," *Comput. Geosci.*, vol. 91, pp. 19–32, Jun. 2016.

[26] D. Wang and C. Xie, "An efficient hybrid sequential approximate optimization method for problems with computationally expensive objective and constraints," *Eng. Comput.*, to be published, doi: 10.1007/s00366-020-01093-w.

[27] X. Song, G. Sun, G. Li, W. Gao, and Q. Li, "Crashworthiness optimization of foam-filled tapered thin-walled structure using multiple surrogate models," *Struct. Multidisciplinary Optim.*, vol. 47, no. 2, pp. 221–231, Feb. 2013.

[28] F. Pan, *Ensemble of Surrogate Models for Lightweight Design of Auto-Body Structure*. Shanghai, China: Shanghai Jiao Tong Univ., 2011.

[29] M. D. Mckay, R. J. Beckman, and W. J. Conover, "A comparison of three methods for selecting values of input variables in the analysis of output from a computer code," *Technometrics*, vol. 42, no. 1, pp. 55–61, Feb. 2000.

[30] Z. C. Li, Y. Jiao, T. W. Deines, Z. J. Pei, and C. Treadwell, "Rotary ultrasonic machining of ceramic matrix composites: Feasibility study and designed experiments," *Int. J. Mach. Tools Manuf.*, vol. 45, nos. 12–13, pp. 1402–1411, Oct. 2005.

[31] G. Lei, X. Chen, and J. Zhu, "Multi-objective sequential optimization method for the design of industrial electromagnetic devices," *IEEE Trans. Magn.*, vol. 48, no. 11, pp. 4538–4541, Nov. 2012.

[32] B. Minasny and A. B. McBratney, "A conditioned latin hypercube method for sampling in the presence of ancillary information," *Comput. Geosci.*, vol. 32, no. 9, pp. 1378–1388, Nov. 2006.

[33] Y. Zhang, W. Li, S. Mao, and Z. Zheng, "Orthogonal arrays obtained by generalized difference matrices with g levels," *Sci. China Math.*, vol. 54, no. 1, pp. 133–143, Jan. 2011.

[34] F. A. C. Viana, G. Venter, and V. Balabanov, "An algorithm for fast optimal latin hypercube design of experiments," *Int. J. Numer. Methods Eng.*, vol. 82, no. 2, pp. 135–156, Oct. 2009.

[35] A. Krogh and J. Vedelsby, "Neural network ensembles, cross validation, and active learning," in *Proc. Adv. Neural Inf. Process. Syst.*, 1995, pp. 231–238.

[36] H. Lin, L. Du, and Y. Liu, "Soft decision cooperative spectrum sensing with entropy weight method for cognitive radio sensor networks," *IEEE Access*, vol. 8, pp. 109000–109008, 2020.

[37] V. Aute, K. Saleh, O. Abdelaziz, S. Azarm, and R. Radermacher, "Cross-validation based single response adaptive design of experiments for kriging metamodeling of deterministic computer simulations," *Struct. Multidisciplinary Optim.*, vol. 48, no. 3, pp. 581–605, Sep. 2013.

[38] *Strength Requirement and Test of Automobile Seats, Their Anchorages and any Bead Restraints*, Standard China GB15083, 2006.

[39] Z. Shan, J. Long, P. Yu, L. Shao, and Y. Liao, "Lightweight optimization of passenger car seat frame based on grey relational analysis and optimized coefficient of variation," *Struct. Multidisciplinary Optim.*, vol. 62, no. 6, pp. 3429–3455, Dec. 2020.

[40] K. Deb, A. Pratap, S. Agarwal, and T. Meyarivan, "A fast and elitist multiobjective genetic algorithm: NSGA-II," *IEEE Trans. Evol. Comput.*, vol. 6, no. 2, pp. 182–197, Apr. 2002.

[41] K. K. Goyal, P. K. Jain, and M. Jain, "Optimal configuration selection for reconfigurable manufacturing system using NSGA II and TOPSIS," *Int. J. Prod. Res.*, vol. 50, no. 15, pp. 4175–4191, Aug. 2012.

JIANGQI LONG is currently a Professor with the College of Mechanical and Electrical Engineering, Wenzhou University. His main research interests include performance analysis, lightweight design theory of car body structure, and structural design and multidisciplinary optimization of auto parts.

YAOQING LIAO was born in 1996. He is currently pursuing the degree with the School of Mechanical and Electrical Engineering, Wenzhou University. His main research interest includes lightweight design of auto parts.

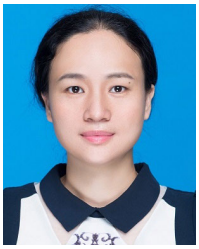

PING YU is currently an Assistant Professor with College of Mechanical and Electrical Engineering, Wenzhou University. Her main research interests include structure optimization design of vehicles and force sensors design for vehicles and robots.